communications materials

A Nature Portfolio journal

Review article

https://doi.org/10.1038/s43246-026-01091-3

# Phase-shift engineered triboelectric nanogenerators for constant-voltage output and efficient energy harvesting



Xinyuan Li[1], Lijiang Yin[1,2], Pengbo Li[1,2] & Jie Wang[1,2]

Triboelectric nanogenerators (TENGs) have emerged as a promising technology for harvesting ambient mechanical energy, their practical deployment has been strongly underpinned by their excellent inherent capabilities for ambient mechanical energy harvesting. Phase-shift engineering, which modulates the phase shifts of electrical outputs from multiple TENG units to achieve continuous constant voltage/current output, further unlocking their full potential and boosting energy utilization efficiency and practicality. This review comprehensively summarizes the fundamental principles of phase-shift engineered TENGs, core design strategies (including inter-unit and intra-unit phase-shift designs, as well as charge excitation-coupled phase-shift approaches), and the efficient energy transport characteristics of CV-TENGs derived from phase-shift engineering. Furthermore, it highlights key challenges like precision manufacturing and environmental robustness, along with future directions of multi-energy coupling and high-end application expansion, providing systematic guidance for high-performance, practical CV-TENG development.

The global pursuit of carbon neutrality, coupled with the rapid advancement of the Internet of Things (IoT), artificial intelligence (AI), and wearable/implantable electronics, has spurred an urgent demand for ubiquitous, portable, and efficient distributed power sources[1–3]. Unlike centralized energy systems, distributed power units excel at harvesting scattered, low-frequency mechanical energy—such as ocean waves, wind, human motion, and vibrations—from the surrounding environment, converting it into usable electricity to support the seamless operation of billions of IoT nodes and miniaturized electronics[4–9].

Triboelectric nanogenerators (TENGs), leveraging the coupling effect of contact electrification and electrostatic induction, have emerged as a highly promising candidate for this critical task. Since their inception[10], TENGs have garnered widespread attention due to their inherent advantages: low manufacturing cost, lightweight structure, high energy conversion efficiency at low frequencies (<5 Hz), and compatibility with diverse mechanical motion forms[11–15]. These distinctive features position TENGs as a core component for self-powered sensors, distributed energy networks, and portable electronic devices, offering substantial potential to address the power supply challenges of next-generation electronic systems. As the demand for stable, continuous, and device-compatible power output grows, TENG technology is undergoing targeted optimization to further enhance its practical applicability and system integration capabilities[16–20].

The development of constant-voltage TENGs (CV-TENGs) represents a transformative advancement in this field, building on the inherent strengths of TENGs to achieve higher performance and broader compatibility[21–24]. The phase-shift design, a key strategy for realizing CV-TENGs, relies on multiple TENG units that generate pulse voltage (PV) signals with consistent frequency and amplitude, modulated through precise structural designs (e.g., angular offset of triboelectric layers, segmented electrodes, or multi-unit stacking). After rectification to unidirectional pulses, these signals are superimposed in parallel, filling gaps between individual pulses to minimize output fluctuations, reduce the crest factor to near 1 (approaching direct current), and ultimately deliver continuous constant-voltage (CV) and constant-current (CC) output. Compared with traditional TENG, the CV-TENG can alter its voltage output signal simply by increasing the number of rectifier bridges. In contrast to the minor energy loss incurred by integrating multiple rectifier bridges, this design significantly reduces the power loss caused by connecting multiple TENGs in series prior to rectification. This innovative design enhances energy storage efficiency and improves compatibility with electronic devices, elevating TENG technology to meet the requirements of practical applications.

Phase-shift engineered TENGs have demonstrated unique advantages that extend the capabilities of traditional TENG systems: (1) CV output that aligns with the input requirements of most commercial electronic devices, simplifying power management by reducing the need for complex voltage regulation circuits; (2) high average power and energy utilization efficiency, enabling continuous operation of electronics without reliance on frequent

[1]Beijing Key Laboratory of High-Entropy Energy Materials and Devices, Beijing Institute of Nanoenergy and Nanosystems, Chinese Academy of Sciences, Beijing, PR China. [2]School of Nanoscience and Technology, University of Chinese Academy of Sciences, Beijing, PR China. e-mail: wangjie@binn.cas.cn

energy storage; and (3) system-level adaptability to cope with the randomness of environmental mechanical energy, ensuring stable performance in diverse scenarios. These features make phase-shift engineered TENGs a key enabler for the next generation of distributed energy systems.

Despite notable advancements, phase-shift engineered TENGs lack a systematic summary of design principles, performance enhancement mechanisms, system integration, and application prospects. This review addresses this gap: it first outlines TENGs' foundational strengths, then explores CV-TENGs' core design strategies and output/stability improvement mechanisms. It also discusses system-level integration (capacitor selection, power management, real-time optimization) and clarifies their role in advancing applications. Finally, it summarizes current progress and future challenges. By summarizing the latest research, this review provides a comprehensive reference to accelerate CV-TENGs' adoption as mainstream distributed energy technologies.

## Fundamental physics of TENGs

In the realm of TENG, basic research has exerted an exceptionally critical influence in translating preliminary experimental phenomena into systematic theoretical frameworks—laying a solid groundwork for its further technological iteration. During the recent decade, the research community has achieved remarkable advancements in unraveling the core mechanisms (such as charge generation, transfer, and dissipation) and physical essence of TENG. This part offers a comprehensive overview of the recent breakthroughs in both the intrinsic theoretical foundations and real-world application pathways of this technology.

### Mechanism of contact electrification

Contact electrification (CE), or triboelectrification, is a ubiquitous phenomenon dating back over 2600 years, yet its fundamental origin—including the identity of charge carriers and transfer mechanisms—has long remained ambiguous. The advent of TENGs has reinvigorated research into CE, driving the development of advanced characterization techniques and theoretical models to unravel its mysteries. In 2014, Zhou et al. used Kelvin Probe Force Microscopy (KPFM) and found that when a metal is in contact with a dielectric material, both the polarity and density of surface charge transfer can be regulated by applying a voltage, thus proving that the charge transfer between the surfaces of the metal and the dielectric material is dominated by electron transfer (Fig. 1a)[25]. In 2018, Xu et al. measured under high-temperature conditions that the charge transfer of inorganic materials exhibits exponential decay with the increase of time. This is consistent with the theory of thermionic emission, revealing that contact electrification between inorganic materials is dominated by electron transfer, and establishing an electron cloud-potential well model applicable to triboelectric charging between any materials (Fig. 1b)[26]. In 2020, Lin et al. discovered by means of KPFM that both electron transfer and ion transfer exist in the solid–liquid triboelectric charging process, and for the first time experimentally verified the new electric double layer model with electron transfer as the dominant mechanism (Fig. 1c)[27]. In the same year, Lin et al. used tapping-mode AFM and KPFM, finding CE electron transfer only in repulsive regions (electron cloud overlap); ≥±2 V bias induces attractive-region tunneling, confirming electron cloud overlap drives solid–solid CE electron transfer. These basic research findings on triboelectric charging provide a solid theoretical foundation for the preparation and optimization of TENGs (Fig. 1d)[28]. These fundamental findings on triboelectric charging—especially the controllability of charge polarity/density and the dominance of electron transfer in solid–solid/solid–liquid systems—lay a critical foundation for phase-shift engineered TENGs. For multi-unit phase modulation, consistent charge transfer across all TENG units ensures uniform amplitude and frequency of pulse signals, which is indispensable for minimizing output fluctuations.

### First-principles of TENGs

The theory of TENGs is based on an equivalent circuit model. The quantification of output power was first achieved in 2017[29], relying heavily on the calculation of displacement current. However, traditional Maxwell's equations are only applicable to describing stationary media and cannot accommodate the medium motion induced by effects such as piezoelectricity and triboelectricity in TENGs. Therefore, they need to be extended, initially by adding the polarization term ($P_s$) generated by medium motion. Subsequent experiments revealed that adding only the polarization term is still insufficient—when TENGs are triggered by sound waves or tapping, they generate electromagnetic radiation, indicating that the impact of medium motion on electromagnetic fields must be systematically considered[30]. From 2021 to 2024, Wang's team derived Maxwell's equations for a mechano-driven media system (MEs-f-MDMS) under the low-speed approximation ($v \ll c$)[31–33].

$$\nabla \cdot D = \rho \tag{1}$$

$$\nabla \cdot B = 0 \tag{2}$$

$$\nabla \times (E + v_r \times B) = -\frac{\partial}{\partial t} B \tag{3}$$

$$\nabla \times (H - v_r \times D) = J + \rho v + \frac{\partial}{\partial t} D \tag{4}$$

This set of equations describes the electromagnetic behavior of moving media in the laboratory coordinate system (*S frame*), introducing the translational velocity of the origin of the reference frame and the rotational velocity of point charges relative to the reference frame, thus making up for the shortcomings of traditional theories. When the system has no translation but only rotation, the equations can be simplified to the form of effective fields, replacing the original electric field ($E$) and magnetic field ($H$) with effective fields ($E_{eff}$) and ($H_{eff}$) that include motion contribution terms such as the Lorentz force. Their propagation, scattering, and other characteristics still comply with the laws of classical equations. This extended set of equations is regarded as the first-principle theory for quantifying TENG output and electromagnetic radiation from moving objects, providing core theoretical support for the performance prediction and system design of TENG. It enables quantitative prediction of the electrical output phase of individual TENG units under dynamic mechanical inputs (e.g., rotation, vibration), guiding the precise design of phase offsets (e.g., angular displacement of triboelectric layers, electrode segmentation) to achieve the optimal phase-shift and stable CV/CC output.

### Working modes of TENGs

TENGs feature four basic operating modes (Fig. 1e): contact-separation, sliding, single-electrode, and freestanding-layer[34–39]. For phase-shift engineered TENGs, contact-separation and freestanding-layer modes are preferred due to their excellent cyclic stability and high energy density—critical for reliable phase modulation across multiple units[40–42]. Structural variants like rotational disk or segmented electrode designs are often adopted to optimize phase synchronization, ensuring consistent amplitude/frequency of outputs from each unit, which lays the foundation for effective phase-shift superposition and stable CV/CC output.

## Phase-shift engineered TENGs

This section summarizes the fundamental principles of phase-shift engineered TENGs, and analyzes all kinds of design strategies, and then presents the resistance load and capacitance load performance of the phase-shift engineered TENG, and gives the strategy of efficient energy transport based on the phase-shift engineered TENG.

### Fundamental principles of phase-shift engineered TENGs

The core principle of phase-shift engineering lies in the coordinated modulation of electrical outputs from multiple TENG units to achieve continuous CV/CC output. For TENG, the equivalent current ($I_{EC}$) and crest factor (CF)—a key indicator of output stability, defined as the ratio of peak

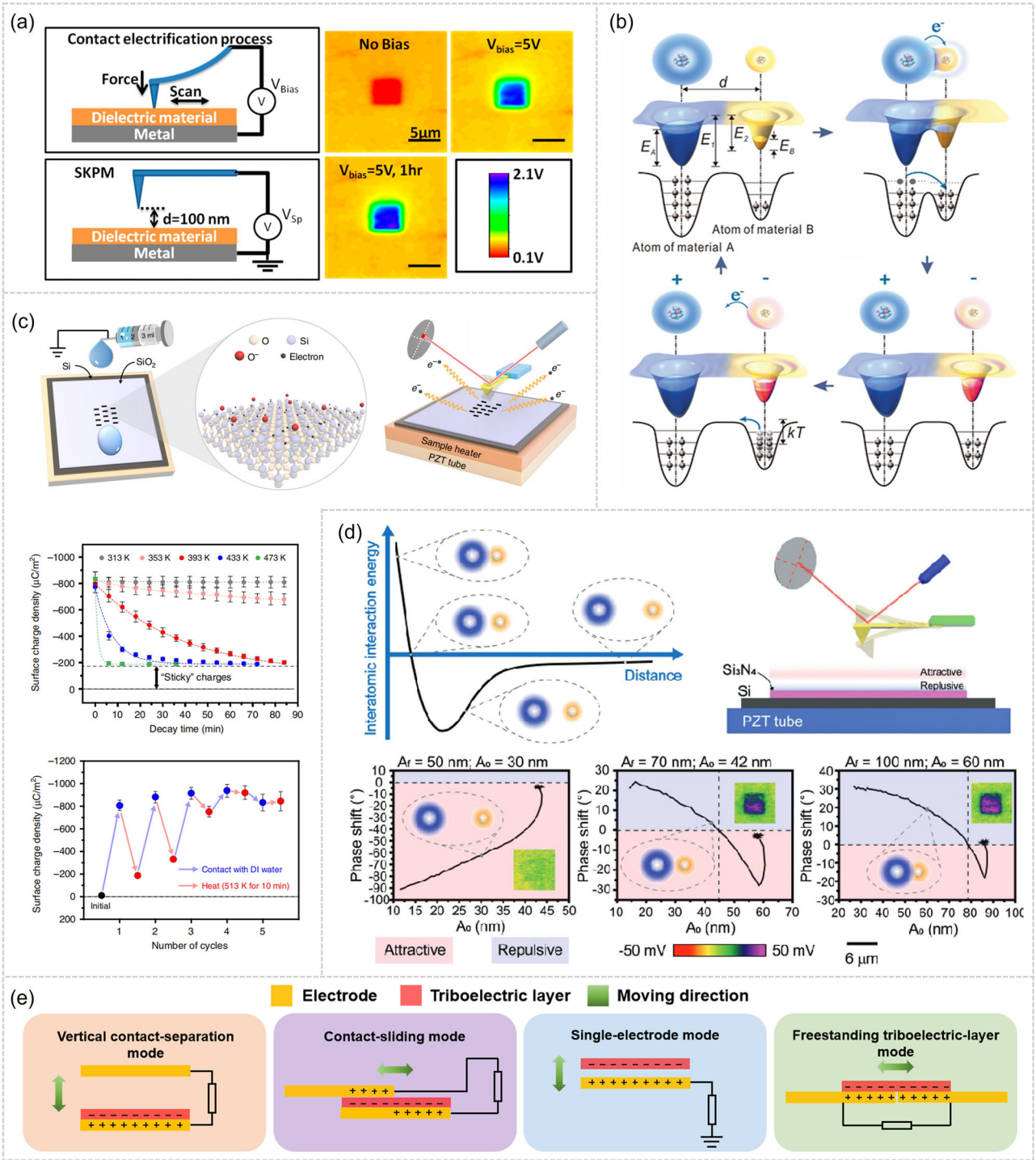


**Fig. 1 | Fundamental physics of TENGs. a** Schematic of manipulating metal-dielectric contact electrification via an applied electric field, as characterized by Kelvin Probe Force Microscopy (KPFM), confirming that electron transfer dominates charge transfer between metal and dielectric surfaces. Reproduced with permission from ref. 25, copyright (American Chemical Society, 2014). **b** Electron-cloud-potential-well model, which explains the electron transfer mechanism during contact electrification between inorganic materials and is applicable to triboelectric charging of any materials. Reproduced with permission from ref. 26, copyright (John Wiley and Sons, 2018). **c** Influence of temperature on contact electrification between deionized water and silicon dioxide: charge transfer exhibits exponential decay with increasing time at high temperatures, consistent with thermionic emission theory and verifying electron transfer as the dominant mechanism in solid–liquid triboelectric charging. Reproduced with permission from ref. 27, copyright (Springer Nature, 2020). **d** Interatomic interaction energy curves, revealing that electron transfer during solid–solid contact electrification only occurs in repulsive regions (electron cloud overlap), while ±2 V bias induces tunneling in attractive regions. Reproduced with permission from ref. 28, copyright (John Wiley and Sons, 2020). **e** Four basic working modes of TENGs: contact-separation, sliding, single-electrode, and freestanding-layer modes, among which contact-separation and freestanding-layer modes are preferred for phase-shift engineered TENGs due to their excellent cyclic stability and high energy density.

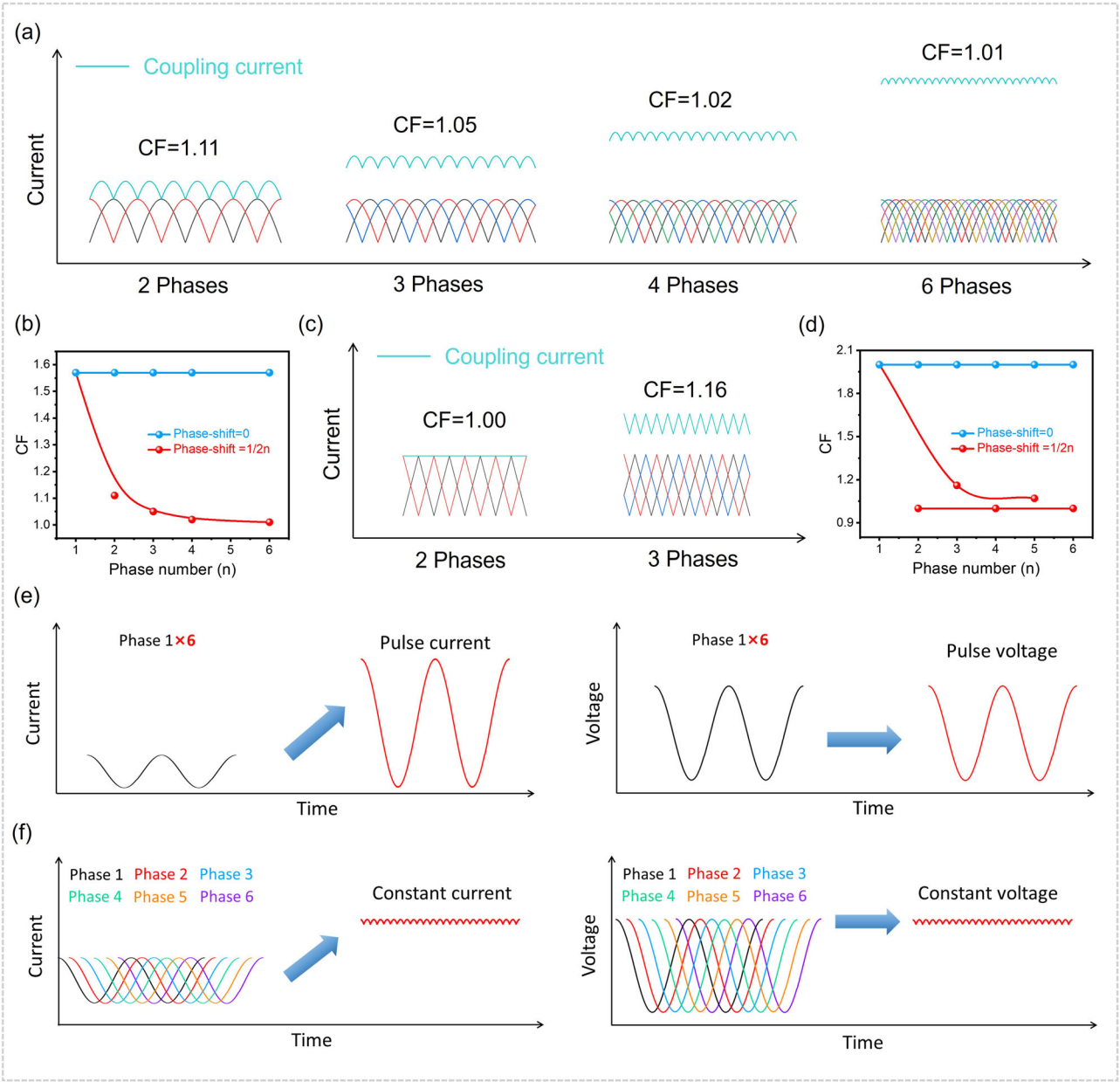


**Fig. 2 | Fundamental principles of phase-shift engineered TENGs. a** Simulated coupling current waveforms of TENGs with different phase numbers (2, 3, 4, 6 phases) under the optimal phase-shift condition (optimal phase-shift = 1/2n, where n = number of phases); the coupling current becomes more stable as the phase number increases. **b** Quantitative relationship between phase number and crest factor (CF, defined as the ratio of peak current to equivalent current): CF decreases significantly with increasing phase number, dropping to 1.01 for 6 phases (approaching ideal constant current, CF = 1). **c** Simulated coupling current waveforms of triangular pulse signals with different phase numbers under optimal phase-shift. **d** Relationship between phase number and CF for triangular waveforms: CF approaches 1.00 as phase number increases, and reaches 1.00 when the phase number is a multiple of 2. **e** Schematic of current and voltage superposition for a conventional pulse-voltage TENG (PV-TENG, 6 units without phase-shift), showing typical discontinuous pulse outputs. **f** Schematic of current and voltage superposition for a phase-shift engineered constant-voltage TENG (CV-TENG, 6 units with optimal phase-shifts): rectified unidirectional pulses of each unit fill the gaps between individual signals, resulting in continuous, smooth constant current (CC) and constant voltage (CV) outputs with minimized fluctuations. Reproduced with permission from ref. 54, copyright (Royal Society of Chemistry, 2022).

current ($I_{Peak}$) to equivalent current—are critical performance parameters, with the mathematical relationship expressed as[43]:

$$I_{EC} = \int_{t}^{t+\Delta t} \frac{Idt}{\Delta t} \tag{5}$$

$$CF = \frac{I_{peak}}{I_{EC}} \tag{6}$$

where $\Delta t$ is the period of the electrical output signal, and $I$ is the instantaneous current. A CF close to 1 indicates an output waveform approaching constant current (CC), which is essential for efficient energy storage and device compatibility.

Figure 2 illustrates the fundamental working mechanism and performance characteristics of phase-shift engineered TENGs. In 2019, Li et al. obtained a low CF output by simulating the superposition of different phase electrical signals of TENG, and proposed the optimal phase-shift for achieving ultra-low CF, which is the optimal phase-shift equal to the reciprocal of twice the number of phases (optimal phase-shift = 1/2n, $n$ = phase number)[43]. Based on Kirchhoff's law and the linear circuit superposition principle, for multi-unit TENGs with consistent amplitude and frequency of pulse outputs, the key to achieving stable CV/CC output is to make the

rectified unidirectional pulse signals of each unit "complement each other" in the time domain, filling the gaps between individual pulses. According to the superposition principle, when the phase difference between adjacent units is set to 1/2n, the time interval between consecutive pulses is minimized ($\Delta t$ = T/(2n), where T is the signal period), ensuring the most uniform signal coverage. Considering that all "physically achievable" waveforms (satisfying the Dirichlet conditions) can be obtained through the transformation of sine functions (superposition, scaling, phase adjustment). The simplest sine function (y = sin x) is used to simulate the waveform of TENG. (The simulated curve of the TENG in the text has rectified from a pulse alternating current to a pulse direct current.) Fig. 2a shows the coupling current waveforms of TENG superposed with different phase numbers (2, 3, 4, 6 phases) under optimal phase-shift conditions. As the number of phases increases, the coupling current becomes more stable, and more phase design achieving the most constant output. Figure 2b quantifies the relationship between phase number and CF: the CF decreases significantly with increasing phase number, dropping to 1.01 for 6 phases, which is nearly ideal CC (CF = 1). Figure 2c, d extends the analysis to triangular waveform outputs. Due to the unique nature of the triangular wave, when the phase number is a multiple of 2, the CF can be reduced to 1.00 (Only match triangular waves). In addition, it still follows the trend that the larger the phase number, the closer the CF gets to 1.00. Figure 2e, f schematically depicts the difference between the conventional pulse-voltage TENG (PV-TENG) and the CV-TENG. Figure 2e exhibits the current and voltage outputs superimposed by six same PV-TENG (1×6 units without phase-shift), showing typical pulse signals. Figure 2f presents the superposition effect of a phase-shift engineered CV-TENG: by integrating six TENG units with optimal phase-shifts, their rectified unidirectional pulses fill the gaps between individual signals, resulting in continuous, smooth, constant current and constant voltage outputs. These results collectively demonstrate that phase-shift engineering minimizes output fluctuations by leveraging the superposition of multi-phase signals, fundamentally resolving the high CF bottleneck of traditional PV-TENGs and enabling efficient energy harvesting and utilization. Although it is known that the CF of TENGs gradually approaches 1 as the number of phases increases, considering that each additional phase requires an extra rectifier, the number of phases for TENGs should be reasonably selected based on actual requirements. Therefore, how to design the phase-shift to obtain a lower CF is crucial. Furthermore, the rule is based on the premise that "all TENG units have consistent amplitude and frequency of output signals". If the environmental mechanical energy is extremely unstable (e.g., severe fluctuation of motion amplitude) or the performance of individual units is inconsistent (e.g., uneven surface charge density), a small deviation from the 1/2n phase-shift may be required to compensate for the signal inconsistency.

## Core design strategies for phase-shift engineered TENGs

Current strategies are categorized into inter-unit phase-shift designs, intra-unit phase-shift designs, and charge excitation-coupled phase-shift designs, with each category adhering to the "phase-shift optimization → signal superposition → CF reduction" logic and sharing distinct commonalities aligned with the above theoretical framework.

**Inter-unit phase-shift designs**. Inter-unit phase-shift designs focus on introducing phase differences between independent TENG units, leveraging spatial layout optimization or external excitation control to ensure each unit's output meets the frequency consistency and optimal phase-shift requirement proposed in Section "Fundamental principles of phase-shift engineered TENGs". Its core advantage lies in flexible scalability—adjusting the number of phases $n$ by increasing units directly follows the "higher $n$ → lower CF" trend validated in Fig. 2.

Natural phase-shift design:. This strategy harnesses inherent asynchrony in environmental mechanical motion (e.g., rotation, fluid flow) to generate phase shifts, avoiding complex active control. Li et al. developed the MRM-TENG for wind energy harvesting, featuring a rotational contact-separation structure with 24 stator electrodes and several rotors. During rotation, natural phase shifts (1/64), corresponding to ($n$ = 32), consistent with (1/2$n$), emerge between units. Each unit is equipped with an independent rectifier to prevent charge cancellation during parallel superposition, achieving a CF of 1.31 (Fig. 3a)[43]. Hong et al. extended this to water flow energy harvesting with the CW-TEH: two asymmetric modules (A/B) on a rotating disc, each with 16 water-filled FEP tubes, offset by 11.25° (module-level) and 22.5° (tube-level) to form 32 units. The phase shift of 1/32 (optimal for $n$ = 16) generates phase-shifted AC signals, which are rectified and superimposed to reduce CF to 1.21 (Fig. 3b)[44].

Mechanical input phase-shift design:. Active phase modulation is achieved via asymmetric structural design of the mechanical excitation system. Dharmasena et al. arranged multiple FSTENG units asymmetrically on a cylindrical holder; a rotor with extended arms excites units at staggered timings (phase shift 1/12, $n$ = 6) via uneven gaps. Rectified and superimposed outputs yield a CF of 1.17, demonstrating precise control over the optimal phase-shift condition (Fig. 3c)[45].

Stacking phase-shift design:. Multiple TENG units are stacked in parallel with controlled inter-layer phase shifts to enhance spatial utilization while increasing $n$. Kim et al. stacked 3 acrylic disks (PTFE-coated Al electrodes, half-immersed in water) with a 120° phase shift (optimal for $n$ = 3), (1/(2 × 3) = 1/6). Three-phase bridge rectification of phase-shifted AC signals produces a stable CC output (Fig. 4a)[46]. Li et al. proposed the CDC-TENG with 3 parallel rotating units (phase shift 1/6, $n$ = 3), achieving an ultra-low CF of 1.05 after superposition (Fig. 4b)[47]. Tao et al. electret TENG adopted multi-layer phase-shift electrodes (stator interdigital electrodes with 1/6 phase shift, $n$ = 3), resulting in a CF of 1.09 (Fig. 4c)[48].

In-plane phase-shift design:. Multiple units are integrated in the same plane via electrode segmentation. The key point is that the number of triboelectric layers is not in the traditional 1:2 ratio with the number of electrodes. Wu et al. rotary disk multi-phase freestanding-electret generators (MFEGs) feature a rotor with PTFE electret sectors and a stator with multi-phase equal-interval electrodes. Specifically, the rotor consists of PTFE electret sectors with equal angular intervals, and the stator is equipped with two-phase interdigital electrodes (phase shift 1/4, $n$ = 2). Therefore, a 2-phase design achieves a CF of 1.09 (Fig. 4d)[49]. Chen et al. MP-TENG segmented traditional electrodes into 4 units (phase shift 1/8, $n$ = 4); rectified and superimposed outputs yield a CF of 1.05 (Fig. 4e)[50].

The commonalities of inter-unit designs rely on phase modulation between independent units, strictly following the (1/2$n$) optimal phase-shift condition. CF decreases with increasing $n$ (ranging from 1.05 to 1.31), and rectification-parallel superposition is indispensable to avoid charge cancellation. These designs excel in scalability and adaptability to low-frequency environmental energy (wind, water flow).

**Intra-unit phase-shift designs**. Intra-unit phase-shift designs realize phase modulation within a single TENG unit by optimizing internal components (electrodes, triboelectric layers), treating a single unit as a multi-phase system to increase $n$ without expanding device volume—directly aligning with Section "Fundamental principles of phase-shift engineered TENGs" "phase number determines CF" principle.

Phase-shift between electrodes and triboelectric layers:. Alternating triboelectric materials or adjusting electrode contact ratios generates phase-shifted signals. Ryu et al. MP-TENG features a rotator with alternating PTFE and MC nylon, and a stator with multiple back electrodes. Each electrode's different contact ratio with the rotator produces phase shifts of 1/10 ($n$ = 5), resulting in a CF of 1.26 after full-wave rectification (Fig. 5a)[51].

Electrodes phase-shift:. Multi-phase electrode design within a unit enables phase modulation. Li et al. D-TENG uses PCB-fabricated multi-phase copper electrodes (covered with FEP film) and a polyester fur rotator; a 4-phase design (phase shift 1/8, $n$ = 4) yields a CF of 1.07 (Fig. 5b)[52]. When

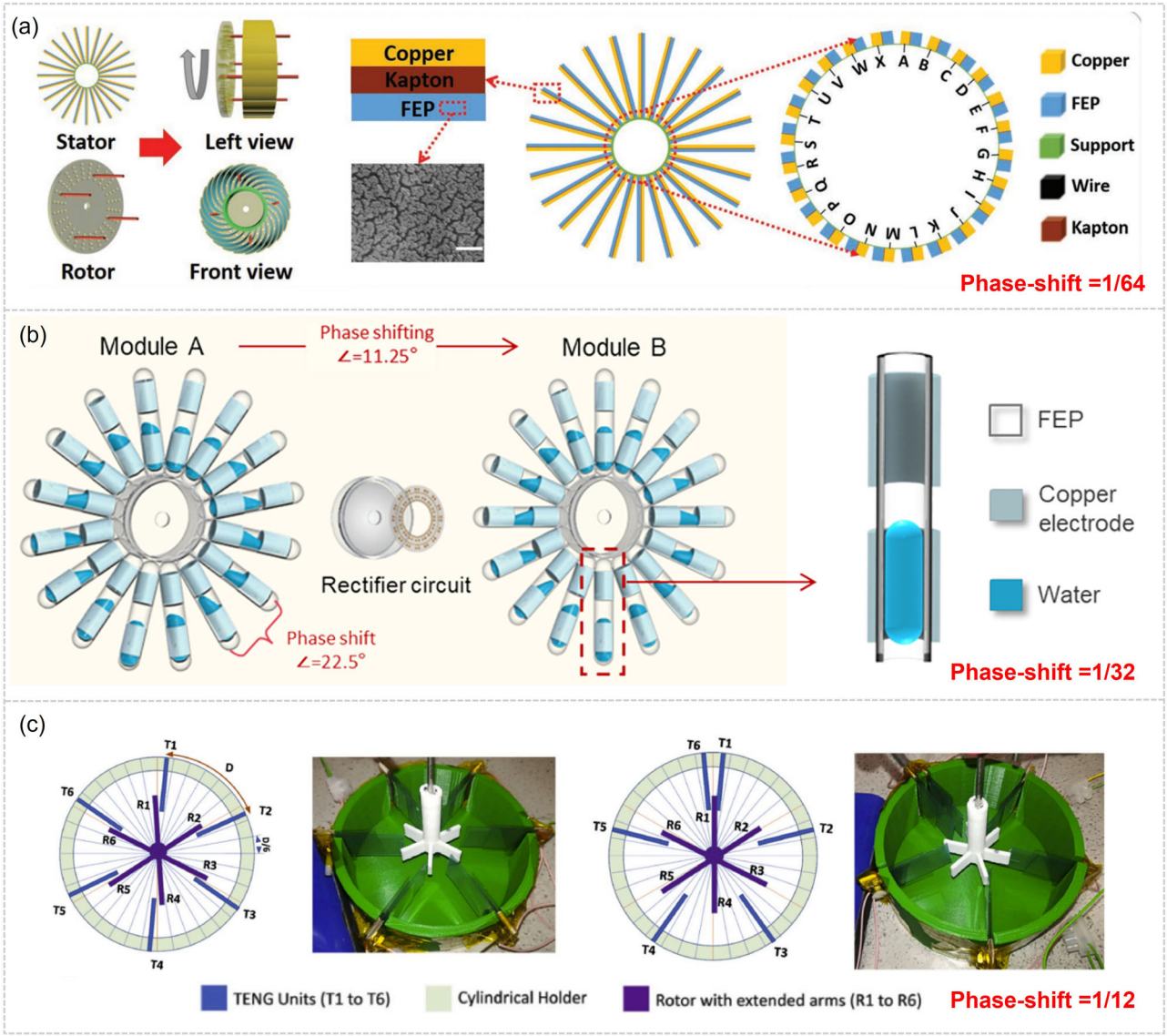


**Fig. 3 | Inter-unit phase-shift designs.** **a** Natural phase-shift design in rotational contact-separation mode: the MRM-TENG for wind energy harvesting consists of 24 stator electrodes and a rotor; natural phase shifts (1/64, corresponding to $n = 32$) emerge between units during rotation. Reproduced with permission from ref. 43, copyright (John Wiley and Sons, 2020). **b** Natural phase-shift design in rotational freestanding mode: the CW-TEH for water flow energy harvesting features two asymmetric modules (A/B) on a rotating disc, each with 16 water-filled FEP tubes; module-level offset of 11.25° and tube-level offset of 22.5° form 32 units with a phase shift of 1/32 (optimal for $n = 16$). Reproduced with permission from ref. 44, copyright (Springer Nature, 2025). **c** Mechanical input phase-shift design in contact-separation mode: multiple FSTENG units are asymmetrically arranged on a cylindrical holder; a rotor with extended arms excites units at staggered timings via uneven gaps, achieving a phase shift of 1/12 ($n = 6$). Reproduced with permission from ref. 45, copyright (Springer Nature, 2020).

extending to 3D structures, Wang et al. cylindrical DC-TENG controls electrode phase shifts via angular offsets (1/6, $n = 3$), achieving a CF of 1.08 at 600 rpm (Fig. 5c)[53].

Triboelectric layers phase-shift:. Staggered arrangement of triboelectric layers introduces phase differences. Li et al. CV-TENG comprises a rotor with 6 radially arrayed, phase-staggered trenches (embedded with dielectric layers) and a stator with 12 electrode sectors. Adjacent electrodes form sub-units with a phase shift of 1/12 ($n = 6$), and superimposed outputs achieve an ultra-low CF of 1.03 (Fig. 5d)[54]. Hu et al. RF-TENG array adopts a multi-layered ring structure with triboelectric layers phase-shifted by 1/12 ($n = 6$), resulting in a CF of 1.07 (Fig. 5e)[55].

The commonalities of intra-unit designs lay in the phase modulation is achieved via structural segmentation within a single unit, effectively increasing $n$ while enhancing spatial utilization. CF values range from 1.03 to 1.26, with planar and 3D configurations both adhering to the $(1/2n)$ optimal phase-shift condition. These designs are ideal for miniaturized and flexible applications.

**Charge excitation-coupled phase-shift design.** This strategy combines charge excitation (active regulation of triboelectric interface charge density) with phase-shift modulation. Compared with direct-current TENG (DC-TENG) that harvests energy via air breakdown, the phase-shift design that relies on electrostatic induction can further enhance its energy output by leveraging the charge pump strategy. The pump-TENG provides stable charge injection to the main-TENG, while the main-TENG adopts phase-shift designs to optimize CF. Hu et al. ECV-TENG consists of an adaptive-contact CV-TENG (ACV-TENG, pump-TENG) and a non-contact CV-TENG (NCV-TENG, main-TENG). The ACV-TENG uses a 1/12 phase shift ($n = 6$) to generate a stable voltage, while the NCV-TENG adopts a 1/2 phase shift between inner/outer rings. Charge injection from the ACV-TENG enhances signal stability, resulting in a CF of 1.04, 80% output retention after 2,000,000

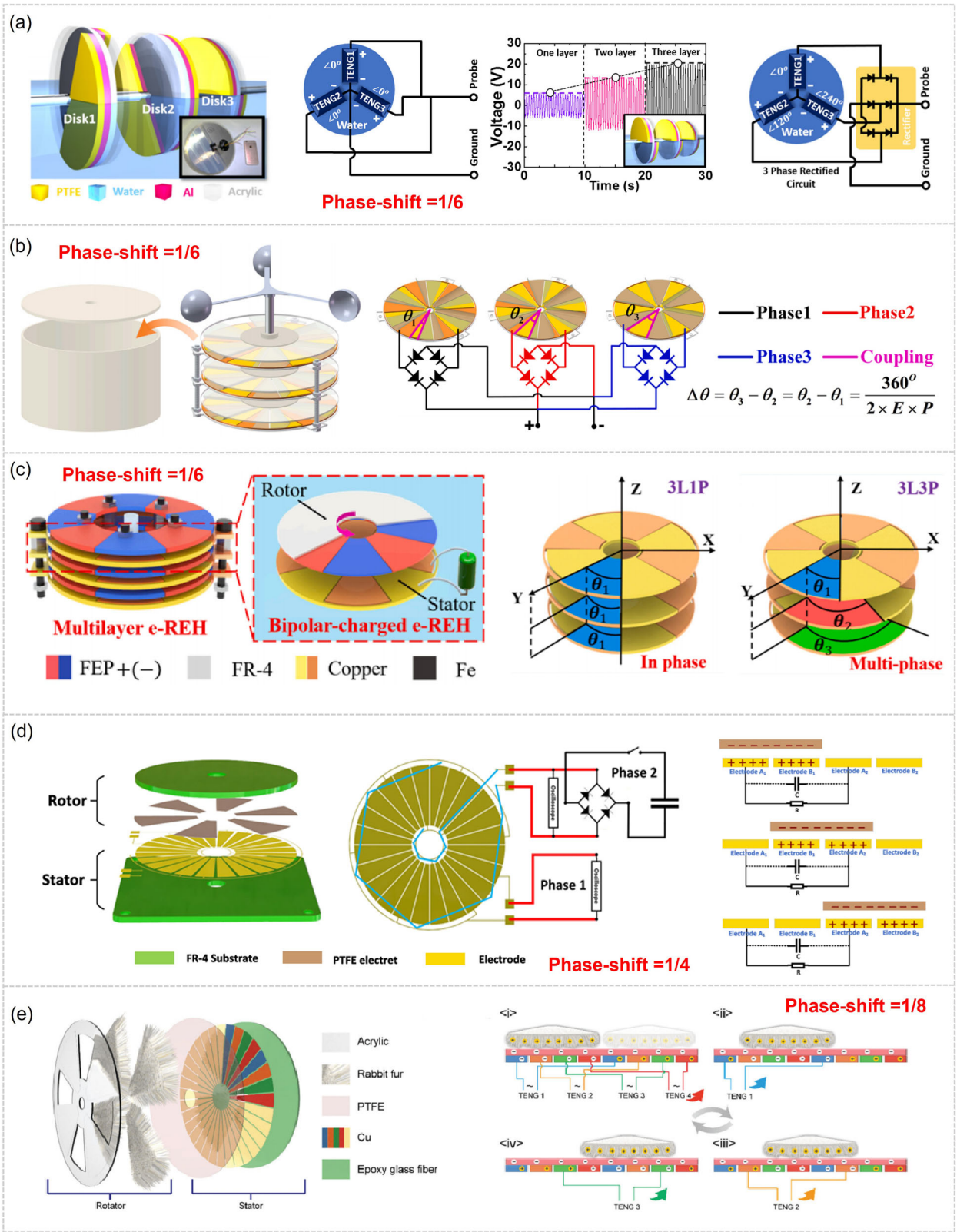


cycles, and humidity resistance up to 90% (Fig. 6a)[56]. Wang et al. humidity-resistant DC-TENG couples a pump-TENG (triboelectric layer phase-shift, 1/8, $n = 4$) with a 3-phase main-TENG (phase shift 1/6, $n = 3$), achieving a CF of 1.23 (Fig. 6b)[53]. Hu et al. EHSS system features a pumping TENG (no phase-shift, charge excitation) and a 2-phase main-TENG, with a CF as low as 1.12 (Fig. 6c)[57].

The commonalities of charge excitation-coupled phase-shift designs integrates dual mechanisms of charge excitation and phase-shift modulation, ensuring multi-phase signals meet the frequency consistency requirement for effective superposition. CF values range from 1.04 to 1.23, with enhanced environmental robustness (humidity/wear resistance) compared to single-mechanism designs. The core physical mechanisms that

**Fig. 4 | Inter-unit phase-shift designs.** **a** Stacking phase-shift design for ocean energy harvesting: 3 acrylic disks (PTFE-coated Al electrodes, half-immersed in water) are stacked with a 120° phase shift (optimal for $n = 3$), and three-phase bridge rectification of phase-shifted AC signals produces a stable CC output. Reproduced with permission from ref. 46, copyright (Springer Nature, 2018). **b** Stacking phase-shift design for wind energy harvesting: the CDC-TENG comprises 3 parallel rotating units with a phase shift of 1/6 ($n = 3$). Reproduced with permission from ref. 47, copyright (Springer Nature, 2022). **c** Stacking phase-shift design for walking energy harvesting: The electret TENG adopts multi-layer phase-shift electrodes (stator interdigital electrodes with 1/6 phase shift, $n = 3$). Reproduced with permission from ref. 48, copyright (Springer Nature, 2023). **d** In-plane phase-shift design (three phases): the rotary disk multi-phase freestanding-electret generator (MFEG) features a rotor with PTFE electret sectors and a stator with two-phase interdigital electrodes (phase shift 1/4, $n = 2$). Reproduced with permission from ref. 49, copyright (Springer Nature, 2021). **e** In-plane phase-shift design (four phases): the MP-TENG segments traditional electrodes into 4 units with a phase shift of 1/8 ($n = 4$). Reproduced with permission from ref. 50, copyright (Springer Nature, 2021).

enable charge excitation-coupled phase-shift designs to improve humidity and wear resistance are as follows. For humidity resistance, the pump-TENG operating in freestanding-layer mode adopts a sliding-mode structure, it is naturally humidity-resistant. Meanwhile, the pump-TENG continuously injects charges into the main-TENG's triboelectric layers, offsetting charge dissipation caused by moisture adsorption (where moisture forms a conductive layer accelerating surface charge leakage) and maintaining stable surface charge density—essential for consistent phase-shifted signal superposition. Additionally, most such systems adopt non-contact or semi-contact structures (e.g., electrostatic induction-based charge injection), reducing direct contact between triboelectric layers and moisture to minimize humidity's impact on contact electrification efficiency. For wear resistance, the charge excitation module boosts output signal amplitude, enabling the main-TENG to achieve the required phase-shifted superposition with lower contact force between triboelectric layers, thereby significantly reducing mechanical wear and material degradation. Furthermore, the decoupling of triboelectric and phase-shift functions—with the pump-TENG handling primary charge generation and the main-TENG focusing on phase modulation—avoids over-reliance on high-frequency, high-intensity contact in single-mechanism designs, extending the device's service life.

To intuitively demonstrate phase-shift designs' TENG performance optimization and schemes differences, the Table summarizes key parameters (structure, phase-shift method, year, power density, CF) of representative TENGs. It shows their CF reduction and average power gains, offering intuitive reference for future research and engineering (Table 1).

## Efficient energy transport based on CV-TENG

If the phase-shift engineered TENG merely appears to convert pulse voltage/current into CV/CC, it is not a wise choice. The fundamental reason lies in the fact that the presence of constant voltage increases the energy transmission efficiency of TENG. Next, we will use CV-TENG to represent the phase-shift engineered TENG to compare its differences with traditional PV-TENG under resistance and capacitance loads.

### The output performance of the CV-TENG under a resistance load

Two types of TENGs (PV-TENG without phase-shift, CV-TENG with phase-shift; Fig. 7a, b) were fabricated using the triboelectric layer phase-shift design in Fig. 5d[54]. Under the same mechanical input, their outputs at different rotating frequencies were tested. PV-TENG showed traditional pulse signals for voltage, while CV-TENG exhibited stable, constant voltage (~1400 V, irrelevant to frequency). Figure 7c showed CV-TENG's maximum average power (53.29 mW at 10 MΩ) was 61.9% higher than PV-TENG's (32.91 mW), with a smaller average-peak power gap (inset). Figure 7d revealed CV-TENG's maximum average power (3.47–53.29 mW at 0.5–4 Hz) was 1.6–1.9 times that of PV-TENG (2.15–33.20 mW) at the same frequencies.

### The output performance of the CV-TENG under a capacitance load

Figure 7e–i illustrate CV-TENG and PV-TENG's output performance and charging mechanisms under a capacitance load. Figure 7e shows CV-TENG charges the capacitor to 989.47 V (vs. 639.92 V for PV-TENG) at 1 Hz, confirming faster charging. Figure 7f reveals energy per cycle peaks with capacitor voltage, highlighting the need for voltage matching. Figure 7g quantifies CV-TENG's higher energy storage (2.28–28.34 mW at 0.5–4 Hz), 1.6–3-fold that of PV-TENG (0.73–14.97 mW), with a 3x boost at 0.5 Hz. Figure 7h, i explain the mechanism difference: PV-TENG retains single-unit pulsed voltage, leading to prolonged capacitor voltage platforms and low energy storage; CV-TENG uses 6-phase superposition via phase-shift design, converting pulse voltage to constant voltage for continuous charging, thus enhancing energy output.

The characteristic differences between resistance and capacitance loads demonstrate that phase-shift engineered TENGs not only achieve the efficient conversion of TENGs' pulsed voltage and current into constant voltage and current but also fundamentally enhance their energy output level, endowing the phase-shift design strategy with greater application value in the TENG energy field.

### Efficient energy transport system based on CV-TENG

Building on the superior output performance of CV-TENGs under resistive and capacitive loads, phase-shift engineering further enables system-level intelligent optimization, constructing a high-efficiency energy transport system that spans energy conversion, storage, transmission, and application. This system fully leverages the stable constant-voltage (CV) output of CV-TENGs, addressing the energy loss and compatibility issues of traditional pulse-voltage TENGs (PV-TENGs) in practical deployment[58]. Figure 8a outlines the overall energy flow framework: environmental mechanical energy (e.g., wind, waves, biomechanics) is converted into stable CV electricity via CV-TENGs, transmitted through low-leakage capacitors, and ultimately powers distributed electronics or self-powered sensors. The core advantage lies in CV-TENG's ability to convert high-entropy, scattered mechanical energy into low-fluctuation electrical energy, laying the foundation for efficient transport. Figure 8b highlights three critical nodes to ensure energy optimization: first, CV-TENG generates continuous CV signals under mechanical excitation, avoiding the voltage plateaus that limit PV-TENG's charging efficiency; second, the CV output enables rapid capacitor charging by eliminating idle periods between pulses; third, a targeted power management module releases stored energy at the optimal threshold, minimizing transmission loss. To realize this, Fig. 8c proposes a universal high-efficiency circuit: two switches ($K_1$, $K_2$) and a temporary capacitor cooperate to store CV-TENG's output energy first, then release it to the power management system cyclically—ensuring a continuous and stable supply for diverse TENG types. Based on this circuit, two power management strategies are developed (Fig. 8d): Type I (discharging to zero) relies on full discharge to maximize energy utilization but only achieves 50% maximum efficiency; Type II (discharging to $U_0$), tailored for CV-TENGs, which retains residual capacitor voltage to expand energy utilization. As shown in Fig. 8e, CV-TENG combined with Type II management achieves efficiency approaching 100% as $U_0$ approaches the TENG voltage (U), with a current practical efficiency of 94.6%—breaking PV-TENG's efficiency bottleneck[57]. Complementing this, the real-time intelligent energy optimization system (RIEOS) dynamically adapts to unstable environmental inputs (Fig. 8f). Through data preprocessing, feature analysis (voltage-time, power-voltage), and iterative feedback, RIEOS adjusts the optimal operating voltage in real time, boosting average power output by ~6.91× compared to conventional systems. This integrated system—combining circuit design, management strategy, and intelligent optimization—ensures CV-TENG's high energy transport efficiency across all links, from device output to practical application. In summary, the CV-TENG-based efficient energy

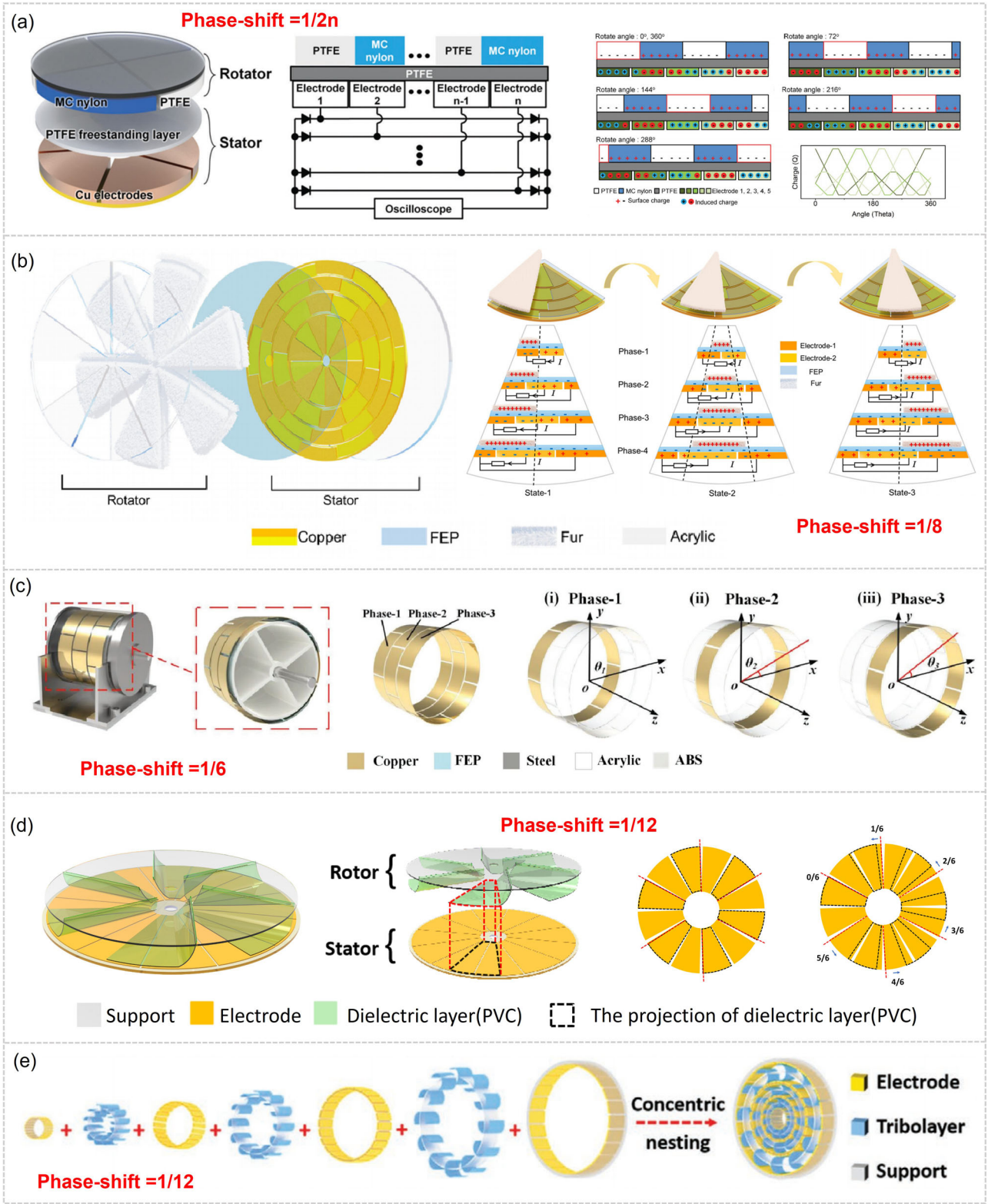


**Fig. 5 | Intra-unit phase-shift designs. a** Phase-shift between electrodes and triboelectric layers in freestanding mode: the MP-TENG has a rotator with alternating PTFE and MC nylon, and a stator with multiple back electrodes. Reproduced with permission from ref. 51, copyright (Royal Society of Chemistry, 2018). **b** Electrode phase-shift in freestanding mode: the D-TENG uses PCB-fabricated 4-phase copper electrodes (covered with FEP film) and a polyester fur rotator. Reproduced with permission from ref. 52, copyright (Royal Society of Chemistry, 2023). **c** Electrode phase-shift in 3D cylindrical structure: the cylindrical DC-TENG controls electrode phase shifts via angular offsets (1/6, $n = 3$). Reproduced with permission from ref. 53, copyright (John Wiley and Sons, 2020). **d** Triboelectric layer phase-shift in freestanding mode: the CV-TENG comprises a rotor with 6 radially arrayed, phase-staggered trenches (embedded with dielectric layers) and a stator with 12 electrode sectors. Reproduced with permission from ref. 54, copyright (Royal Society of Chemistry, 2022). **e** Triboelectric layer phase-shift in multi-layer 3D structure: the RF-TENG array adopts a multi-layered ring structure with triboelectric layers phase-shifted by 1/12 ($n = 6$). Reproduced with permission from ref. 55, copyright (John Wiley and Sons, 2021).

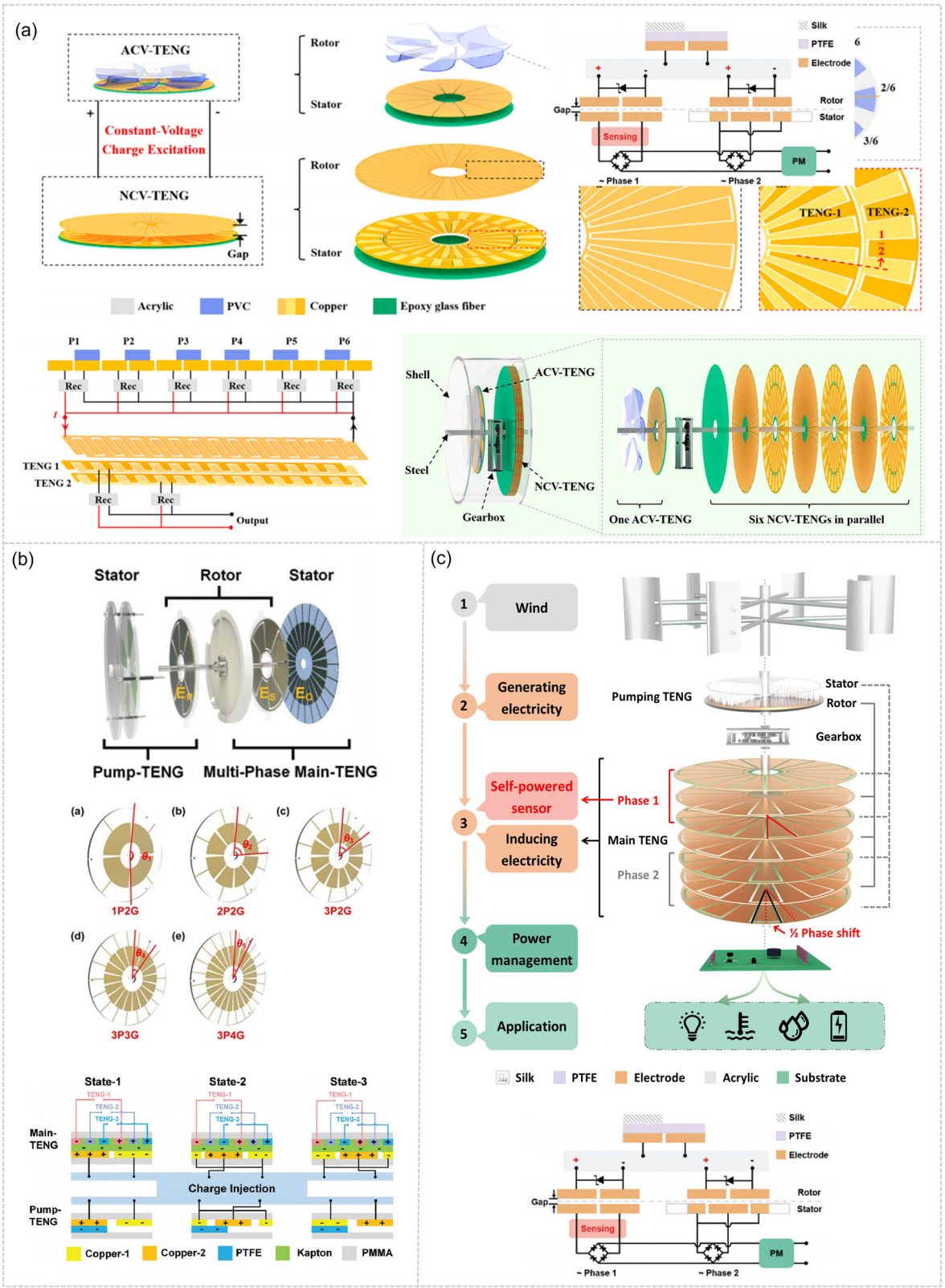


**Fig. 6 | Charge excitation based on phase-shift TENGs. a** ECV-TENG system: the pump-TENG (ACV-TENG) uses triboelectric layer phase-shift (1/12, $n = 6$) to generate stable voltage, while the main-TENG (NCV-TENG) adopts electrode phase-shift (1/2 between inner/outer rings). Reproduced with permission from ref. 56, copyright (Springer Nature, 2023). **b** Humidity-resistant DC-TENG: the pump-TENG uses triboelectric layer phase-shift (1/8, $n = 4$) for charge excitation, and the main-TENG is a 3-phase system with electrode-triboelectric layer phase-shift (1/6, $n = 3$). Reproduced with permission from ref. 53, copyright (John Wiley and Sons, 2023). **c** EHSS wind harvesting system: the pump-TENG (no phase-shift) provides charge excitation, and the main-TENG is a 2-phase system with electrode phase-shift. Reproduced with permission from ref. 57, copyright (Springer Nature, 2024).

**Table 1 | The development of the phase-shift engineered TENG**

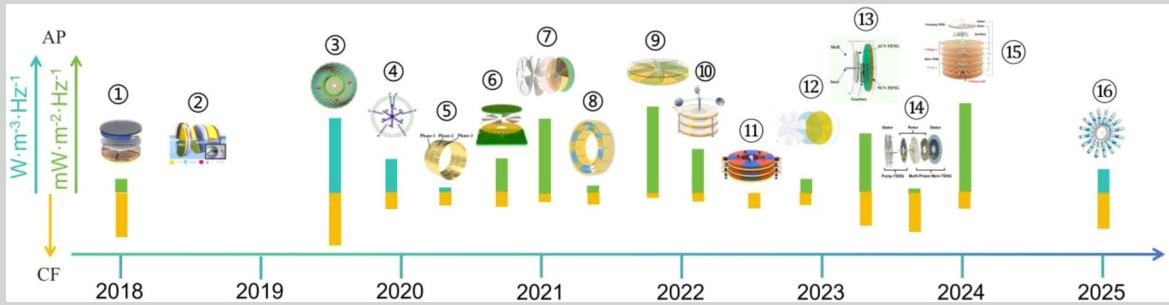


| No | Phase-shift Strategy | Year | Average power | CF | References |
|---|---|---|---|---|---|
| 1 | Phase-shift between electrode and triboelectric layer in-plane | 2018 | 40.6 (mW m$^{-2}$ Hz$^{-1}$) | 1.26 | 51 |
| 2 | Stacking phase-shift | 2018 | - | - | 46 |
| 3 | Natural phase-shift | 2020 | 4.42 (W m$^{-3}$ Hz$^{-1}$) | 1.31 | 43 |
| 4 | Mechanical input phase-shift | 2020 | 2.0 (W m$^{-3}$ Hz$^{-1}$) | 1.10 | 45 |
| 5 | Electrode phase-shift in 3D structure | 2020 | 0.29 (W m$^{-3}$ Hz$^{-1}$) | 1.08 | 62 |
| 6 | Phase-shift design in-plane | 2021 | 98 (mW m$^{-2}$ Hz$^{-1}$) | 1.09 | 49 |
| 7 | Phase-shift design in-plane | 2021 | 222 (mW m$^{-2}$ Hz$^{-1}$) | 1.05 | 50 |
| 8 | Triboelectric layer phase-shift in 3D structure | 2021 | 22.45 (mW m$^{-2}$ Hz$^{-1}$) | 1.07 | 55 |
| 9 | Stacking phase-shift | 2022 | 133 (mW m$^{-2}$ Hz$^{-1}$) | 1.05 | 47 |
| 10 | Triboelectric layer phase-shift in-plane | 2022 | 254 (mW m$^{-2}$ Hz$^{-1}$) | 1.03 | 54 |
| 11 | Electrode phase-shift in-plane | 2023 | 43.1 (mW m$^{-2}$ Hz$^{-1}$) | 1.07 | 52 |
| 12 | Stacking phase-shift | 2023 | - | 1.09 | 48 |
| 13 | Pump-TENG: Triboelectric layer phase-shift in-plane<br>Main-TENG: Electrode phase-shift in-plane | 2023 | 173.5 (mW m$^{-2}$ Hz$^{-1}$) | 1.2 | 56 |
| 14 | Pump-TENG: Triboelectric layer phase-shift in-plane<br>Main-TENG: Electrode phase-shift in-plane | 2023 | 18 (mW m$^{-2}$ Hz$^{-1}$) | 1.23 | 53 |
| 15 | Pump-TENG: No phase-shift in-plane<br>Main-TENG: Electrode phase-shift in-plane | 2024 | 262 (mW m$^{-2}$ Hz$^{-1}$) | 1.1 | 57 |
| 16 | Natural phase-shift | 2025 | 1.4 (W m$^{-3}$ Hz$^{-1}$) | 1.21 | 44 |

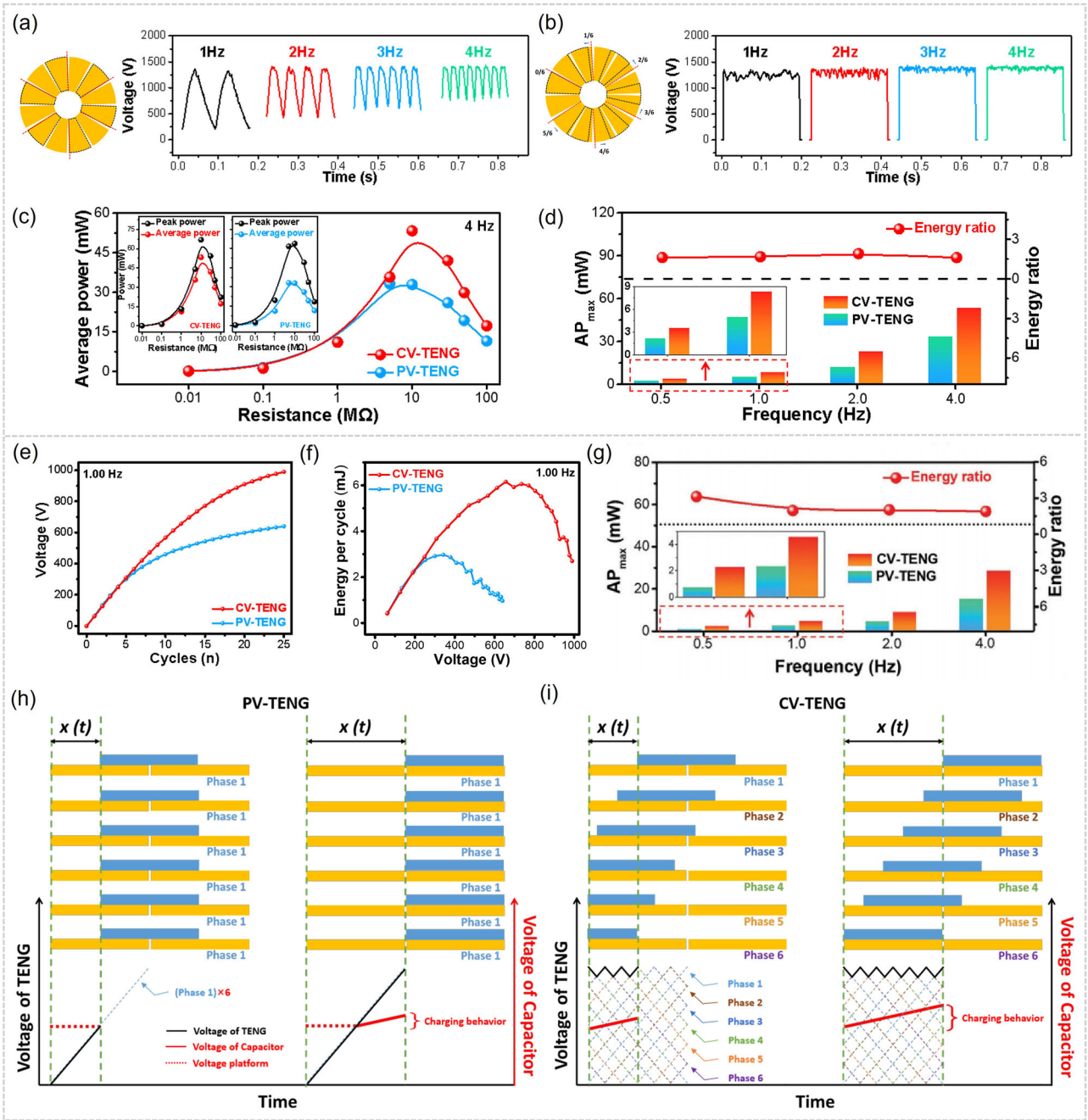


**Fig. 7 | The output performance of the CV-TENG under a resistance load and a capacitance load.** Reproduced with permission from ref. 54, copyright (Royal Society of Chemistry, 2022). The illustration, voltage outputs of **a** a PV-TENG and **b** a CV-TENG under different frequency. **c** A comparison of the average power between a CV-TENG and PV-TENG over a resistance load range from 0.01 to 100 MΩ; inset: a comparison of the average power and peak power between a CV-TENG (left) and PV-TENG (right) under resistance loads. **d** The maximum average power (AP) of a CV-TENG and PV-TENG and their energy ratios at different frequencies. **e** The charging voltage of the capacitor. **f** The energy flowing to the capacitor per cycle versus the voltage of the capacitor when charged by the CV-TENG and PV-TENG. **g** The maximum average power (AP) of the CV-TENG and PV-TENG under a capacitance load and their energy ratios at different frequencies. Schematic illustrations of the charging principles of the (h) PV-TENG and (i) CV-TENG under a capacitance load.

transport system resolves traditional TENGs' key limitations through synergistic device-level phase-shift design and system-level optimization. Its high efficiency, stability, and adaptability provide a reliable technical framework for CV-TENG's deployment in distributed energy networks, self-powered sensors, and portable electronics.

## The application of phase-shift CV-TENG

Benefiting from stable CV/CC output, high energy transport efficiency, and adaptability to diverse mechanical energy sources, phase-shift engineered CV-TENGs have been widely explored in practical scenarios (Fig. 9). These applications fully leverage the core advantages of CV-TENGs in low-frequency energy harvesting and direct device compatibility.

In wind energy harvesting (Fig. 9a)[43], CV-TENGs are integrated with rotational structures to convert low-frequency wind energy into stable electricity. They can directly power small electronic devices (e.g., LEDs, electronic watches) or store energy in batteries for off-grid use. For intelligent environmental monitoring, CV-TENGs combined with charge excitation phase-shift design enable self-powered wind sensors (Fig. 9b)[56,57], which not only harvest wind energy to sustain their own operation but also realize real-time wind speed sensing through signal

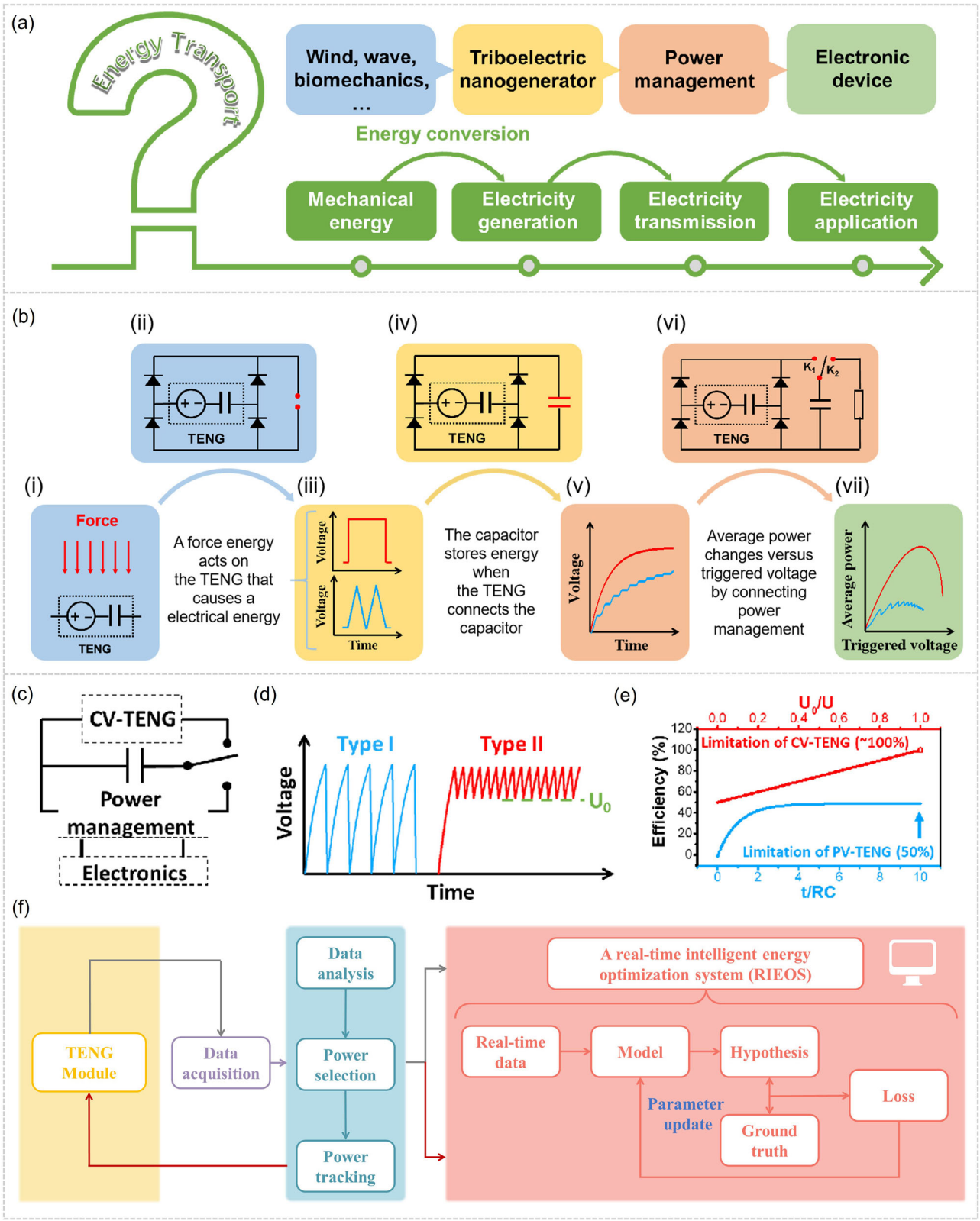


**Fig. 8 | Efficient energy transport system based on CV-TENG.** Reproduced with permission from ref. 58, copyright (Royal Society of Chemistry, 2024). **a** Schematic diagram of energy transport in TENG-based power units from environmental mechanical energy to distributed energy application. **b** Schematic diagram of efficient energy transport in TENG-based power units to maintain efficient electricity supply and transmission at every node and link. **c** Universal circuit connections for obtaining a highly efficient CV-TENG. **d** Two methods of power management for the CV-TENG (Type I: discharging to zero; Type II: discharging to $U_0$). **e** Changes in energy-output efficiency versus $U_0/U$ and t/RC. **f** Flow diagram of the underlying logic for the RIEOS.


**Fig. 9 | The application of the CV-TENG. a** Harvesting the wind energy to direct power to small electronics or store the energy in a battery. Reproduced with permission from ref. 43, copyright (John Wiley and Sons, 2020). **b** Self-powered wind senser by charge excitation phase-shift TENGs. Reproduced with permission from ref. 56, copyright (Springer Nature, 2023). **c** Water flow energy harvesting to power sensors. Reproduced with permission from ref. 53, copyright (John Wiley and Sons, 2023). **d** The CV-TENG was placed in the bottom of human shoes and used to collect human walking, running, and other sports energy. Reproduced with permission from ref. 48, copyright (Springer Nature, 2023). **e** CV-TENG in smart green travel. Reproduced with permission from ref. 50, copyright (Springer Nature, 2021). **f** The self-powered smart feedback system for air circulation. Reproduced with permission from ref. 51, copyright (Royal Society of Chemistry, 2018). **g** CV-TENG providing stable electricity for the optical computing chip in electromagnetic environments. Reproduced with permission from ref. 52, copyright (Royal Society of Chemistry, 2023).

processing, demonstrating dual functionality in energy harvesting and sensing.

In water flow energy harvesting (Fig. 9c)[53], waterproof and corrosion-resistant CV-TENG configurations are deployed to capture energy from ocean waves, river currents, or industrial water flows. Their stable output ensures a reliable power supply for underwater sensors (e.g., temperature, pressure sensors) and marine monitoring equipment, addressing the power shortage challenge in aquatic environments.

For human-centric energy harvesting (Fig. 9d)[48], miniaturized and flexible CV-TENGs are integrated into the soles of shoes or wearable devices to collect mechanical energy from human motion (walking, running, etc.). The continuous CV output efficiently powers portable electronics (e.g., smartwatches, calculators) and self-powered sensor networks, reducing reliance on disposable batteries. This application is further extended to smart green travel (Fig. 9e)[50], where CV-TENGs installed on bicycles or electric vehicles harvest rotational or vibrational energy to power cyclo-computers, navigation devices, or auxiliary systems, enhancing the energy sustainability of travel tools.

In building and environmental regulation (Fig. 9f)[51], CV-TENGs are integrated into ventilation systems to form self-powered smart feedback loops. They harvest energy from air flow or structural vibrations, powering sensors that monitor air quality and airflow speed, and dynamically adjusting ventilation intensity based on real-time data, achieving energy-efficient building management.

Notably, CV-TENGs exhibit unique advantages in special electromagnetic environments (Fig. 9g)[52]. Their triboelectric-based energy conversion mechanism is less susceptible to electromagnetic interference, making them ideal power sources for optical computing chips and anti-interference sensing systems. The stable CV output ensures the reliable operation of precision electronic components in complex electromagnetic

fields, expanding the application scope of TENGs beyond conventional scenarios. In summary, the applications of CV-TENG overlap with those of traditional TENGs[59–61]; meanwhile, owing to its CV/CC output characteristics, it exhibits broader application advantages.

## Outlook

Phase-shift engineered CV-TENGs represent a crucial step forward for triboelectric energy harvesting technology toward practical application. By ingeniously coordinating the phase outputs of multiple TENG units, they effectively transform the traditional pulsed voltage/current output into stable, continuous CV/CC output with a crest factor approaching unity. This fundamental advancement not only simplifies the power management interface with electronic devices but also significantly enhances energy transmission and storage efficiency, demonstrating immense potential in various environmental energy harvesting scenarios such as wind, water, wearable devices, and smart systems. However, several scientific and engineering challenges must be overcome to transition CV-TENGs from laboratory prototypes to large-scale commercialization and widespread deployment. In-depth exploration of the following directions will be the focus of future research:

### Precision phase control for large-scale integration

The core challenge in building large-scale, high-power-output CV-TENG arrays lies in ensuring long-term, stable, and precise phase synchronization among numerous units. Minute assembly errors, material wear, or environmental vibrations can disrupt phase consistency, leading to degraded output stability. Future research should focus on:

**Self-synchronizing and fault-tolerant designs**. The phase control mechanisms to be explored do not rely on external precision calibration. For instance, passive self-synchronizing structures based on mechanical interlocking, electrostatic coupling, or magnetic coupling can be constructed, with such structures enabling individual units to adjust their phases in an adaptive manner. Simultaneously, circuit architectures and management algorithms with a certain degree of phase fault tolerance can be established to alleviate excessive reliance on manufacturing precision.

**Phase adaptation in dynamic environments**. Natural energy sources (e.g., ocean waves, irregular gusts) are inherently stochastic and unstable. The phase response characteristics of CV-TENG systems under such non-steady inputs are to be systematically investigated. Novel structures capable of harnessing this randomness to yield beneficial "natural phase shifts" are to be devised, alongside real-time feedback systems that dynamically adjust operating parameters for the maintenance of optimal output.

### Extreme environmental adaptability and scalable manufacturing processes

The practical application scenarios for CV-TENGs are often harsh, placing high demands on their environmental robustness.

**Enhancing environmental tolerance**. For extreme conditions such as high humidity (>90% RH), wide temperature ranges (−40 °C–85 °C), seawater corrosion, and sand/dust, it is necessary to develop long-lasting encapsulation technologies (e.g., atomic layer deposition, high-performance polymer encapsulation), novel hydrophobic/anti-fouling interface materials, and strategies combined with charge pumping (e.g., the ECV-TENG mentioned in the document) to maintain high performance. For special applications like deep-sea or aerospace, the impact of extreme physical conditions like high pressure or vacuum must also be considered.

**Low-cost, scalable manufacturing**. The fabrication of many high-performance CV-TENGs currently involves precision machining, which can be costly. Promoting manufacturing processes suitable for industrial production is crucial. For example, the implementation of high-volume, consistent manufacturing techniques—rooted in 3D printing (especially suited for complex 3D structures), roll-to-roll printing, laser micromachining, or injection molding—is a core priority. Meanwhile, the exploration of designs compatible with standard MEMS or PCB processes serves as an effective pathway to achieve significant production cost reduction.

### Multi-energy coupling and intelligent system integration

A single energy harvesting mode struggles to cope with the complex and variable real-world environment. The synergy between CV-TENGs and other energy harvesting technologies will open new dimensions.

**Hybrid energy harvesting systems**. CV-TENGs are to be integrated with solar cells, electromagnetic generators, piezoelectric nanogenerators, and other complementary energy harvesters, for the construction of hybrid harvesting systems that span broad frequency bands and multiple physical fields. Concurrently, efficient multi-energy interface circuits and cooperative energy management strategies, including intelligent switching or hybridization based on maximum power point tracking, are to be prioritized to realize a stable power supply across all weather conditions and application scenarios.

**System-level intelligence and efficient energy management**. A shift of focus beyond standalone devices allows for the establishment of more intelligent energy Internet of Things (IoT) nodes. Real-time intelligent energy optimization systems, as mentioned in this document, are integrated into these nodes, with machine learning algorithms applied to predict optimal operating points based on historical data and real-time inputs for the realization of dynamic load matching adjustments. Furthermore, advanced power management strategies like non-zero threshold discharging will be developed, which push the system-level energy utilization efficiency toward its theoretical limit (approaching 100%) and support on-demand energy distribution as well as wireless transmission functions.

### Expansion into high-end application scenarios and multi-functional integration

Leveraging their unique advantages, such as anti-electromagnetic interference, high efficiency at low frequencies, and a wide choice of materials, CV-TENGs are poised to enter frontier areas where traditional power technologies are difficult to apply.

**Powering emerging fields**. For implantable and wearable medical devices, CV-TENGs can harvest energy from body motion, heartbeat, or even blood flow to power long-term monitoring sensors, reducing or eliminating the need for battery replacement surgery. Their environmental resilience and fuel-free nature are highly attractive for deep-sea in-situ detectors or space probes. Furthermore, they can provide self-powered solutions for distributed IoT nodes and structural health monitoring sensor networks.

**Integrated energy harvesting-sensing systems**. The output signal of a CV-TENG inherently carries rich information about the mechanical excitation source (e.g., frequency, amplitude, phase). Future efforts should focus on developing dual-function or even multi-function systems where the device simultaneously acts as a highly sensitive self-powered sensor. For example, the demonstrated wind speed and direction sensors allow for extension to diverse application domains, including vibration monitoring, posture recognition, and tactile perception, with the realization of closed-loop intelligent systems characterized by the principle of "sensing enables powering, and powering enables utility". Such systems provide profound empowerment to smart cities, human-machine interaction, and Industry 4.0 initiatives.

In summary, the future development of phase-shift engineered CV-TENGs will be a process of deep multidisciplinary integration involving

device physics, materials science, precision manufacturing, circuit design, and system integration. By addressing the aforementioned challenges, CV-TENGs have the potential to evolve from a promising energy harvesting technology into a foundational power solution supporting distributed, self-powered electronic systems in the era of the Internet of Everything.

Received: 27 November 2025; Accepted: 23 January 2026;
Published online: 02 February 2026

## References

1. Chen, J. & Wang, Z. L. Reviving vibration energy harvesting and self-powered sensing by a triboelectric nanogenerator. *Joule* **1**, 480–521 (2017).
2. Wang, Z. L. Catch wave power in floating nets. *Nature* **542**, 159–160 (2017).
3. Gu, H. et al. A battery-free wireless tactile sensor for multimodal force perception. *Adv. Funct. Mater.* **34**, 2410661 (2024).
4. Wang, X. D., Song, J. H., Liu, J. & Wang, Z. L. Direct-current nanogenerator driven by ultrasonic waves. *Science* **316**, 102–105 (2007).
5. Ji, M. et al. Machine learning–assisted triboelectric nanogenerator technology for intelligent sports. *Sci. Adv.* **11**, eadz3515 (2025).
6. Jiang, T. et al. Robust swing-structured triboelectric nanogenerator for efficient blue energy harvesting. *Adv. Energy Mater.* **10**, 2000064 (2020).
7. Lei, H. et al. Self-assembled porous-reinforcement microstructure-based flexible triboelectric patch for remote healthcare. *Nano-Micro Lett.* **15**, 109 (2023).
8. Li, H. et al. A contact-electro-catalytic cathode recycling method for spent lithium-ion batteries. *Nat. Energy* **8**, 1137–1144 (2023).
9. Lu, X. et al. Triboelectric sensor gloves for real-time behavior identification and takeover time adjustment in conditionally automated vehicles. *Nat. Commun.* **16**, 1080 (2025).
10. Fan, F. R., Tian, Z. Q. & Wang, Z. L. Flexible triboelectric generator!. *Nano Energy* **1**, 328–334 (2012).
11. Chen, J. et al. Stackable direct current triboelectric-electromagnetic hybrid nanogenerator for self-powered air purification and quality monitoring. *Adv. Energy Mater.* **13**, 2203689 (2023).
12. Chen, J., Guo, H., Hu, C. & Wang, Z. L. Robust triboelectric nanogenerator achieved by centrifugal force induced automatic working mode transition. *Adv. Energy Mater.* **10**, 2000886 (2020).
13. Chen, P. et al. Super-durable, low-wear, and high-performance fur-brush triboelectric nanogenerator for wind and water energy harvesting for smart agriculture. *Adv. Energy Mater.* **11**, 2003066 (2021).
14. Chen, P. et al. Achieving high power density and durability of sliding mode triboelectric nanogenerator by double charge supplement strategy. *Adv. Energy Mater.* **12**, 2201813 (2022).
15. Li, Y. et al. Visualization and standardized quantification of surface charge density for triboelectric materials. *Nat. Commun.* **15**, 6004 (2024).
16. Fu, J. J. et al. Achieving ultrahigh output energy density of triboelectric nanogenerators in high-pressure gas environment. *Adv. Sci.* **7**, 2001757 (2020).
17. Gao, Y. et al. Achieving high-efficiency triboelectric nanogenerators by suppressing the electrostatic breakdown effect. *Energy Environ. Sci.* **16**, 2304–2315 (2023).
18. Gbadam, G. S. et al. Direct current generation in triboelectric nanogenerators through ionic dynamics and electrode polarization effects. *Nat. Commun.* **16**, 9540 (2025).
19. Li Y. et al. Improved output performance of triboelectric nanogenerator by fast accumulation process of surface charges. *Adv. Energy Mater.* **11**, 2100050 (2021).
20. Xu, G. et al. Self-powered electrotactile textile haptic glove for enhanced human-machine interface. *Sci. Adv.* **11**, eadt0318 (2025).
21. Liu, D. et al. A constant current triboelectric nanogenerator arising from electrostatic breakdown. *Sci. Adv.* **5**, eaav6437 (2019).
22. Zhao, Z. H. et al. Rationally patterned electrode of direct-current triboelectric nanogenerators for ultrahigh effective surface charge density. *Nat. Commun.* **11**, 6186 (2020).
23. Zhao, Z. H. et al. Selection rules of triboelectric materials for direct-current triboelectric nanogenerator. *Nat. Commun.* **12**, 4686 (2021).
24. Zhao, Z. H. & Wang, J. Advances in interfacial electrostatic energy harvesting via direct current triboelectric nanogenerators. *Adv. Energy Mater.* **15**, 2502544 (2025).
25. Zhou, Y. S. et al. Manipulating nanoscale contact electrification by an applied electric field. *Nano Lett.* **14**, 1567–1572 (2014).
26. Xu, C. et al. On the electron-transfer mechanism in the contact-electrification effect. *Adv. Mater.* **30**, 1706790 (2018).
27. Lin, S., Xu, L., Wang, A. & Wang, Z. L. Quantifying electron-transfer in liquid-solid contact electrification and the formation of electric double-layer. *Nat. Commun.* **11**, 399 (2020).
28. Lin, S., Xu, C., Xu, L. & Wang, Z. L. The overlapped electron-cloud model for electron transfer in contact electrification. *Adv. Funct. Mater.* **30**, 1909724 (2020).
29. Wang, Z. L. On Maxwell's displacement current for energy and sensors: the origin of nanogenerators. *Mater. Today* **20**, 74–82 (2017).
30. Chen, C. et al. Micro triboelectric ultrasonic device for acoustic energy transfer and signal communication. *Nat. Commun.* **11**, 4143 (2020).
31. Wang, Z. L. General solutions of the Maxwell's equations for a mechano-driven media system (MEs-f-MDMS). *J. Phys. Commun.* **8**, 115004 (2024).
32. Wang, Z. L. The Maxwell's equations for a mechano-driven media system (MEs-f-MDMS). *Adv. Phys.-X* **9**, 2354767 (2024).
33. Wang, Z. L. On the expanded Maxwell's equations for moving charged media system – General theory, mathematical solutions and applications in TENG. *Mater. Today* **52**, 348–363 (2022).
34. Pang, H. et al. Segmented swing-structured fur-based triboelectric nanogenerator for harvesting blue energy toward marine environmental applications. *Adv. Funct. Mater.* **31**, 2106398 (2021).
35. Qin, S. et al. Triboelectric sensor with ultra-wide linear range based on water-containing elastomer and ion-rich interface. *Nat. Commun.* **15**, 10640 (2024).
36. Wang, H. M., Xu, L., Bai, Y. & Wang, Z. L. Pumping up the charge density of a triboelectric nanogenerator by charge-shuttling. *Nat. Commun.* **11**, 4203 (2020).
37. Wang, J. et al. Sustainably powering wearable electronics solely by biomechanical energy. *Nat. Commun.* **7**, 12744 (2016).
38. Wang, J. et al. Achieving ultrahigh triboelectric charge density for efficient energy harvesting. *Nat. Commun.* **8**, 88 (2017).
39. Wei, X. et al. Hybridized mechanical and solar energy-driven self-powered hydrogen production. *Nano-Micro Lett.* **12**, 88 (2020).
40. Zhu, G. et al. A shape-adaptive thin-film-based approach for 50% high-efficiency energy generation through micro-grating sliding electrification. *Adv. Mater.* **26**, 3788–3796 (2014).
41. Zi, Y. L. et al. Effective energy storage from a triboelectric nanogenerator. *Nat. Commun.* **7**, 10987 (2016).
42. Zi, Y. L. et al. Standards and figure-of-merits for quantifying the performance of triboelectric nanogenerators. *Nat. Commun.* **6**, 8376 (2015).
43. Li, X. Y. et al. Long-lifetime triboelectric nanogenerator operated in conjunction modes and low crest factor. *Adv. Energy Mater.* **10**, 1903024 (2020).
44. Hong, H. et al. Constant-current water-tube triboelectric energy harvester for low-frequency rotational energy harvesting. *Chem. Eng. J.* **509**, 161340 (2025).
45. Dharmasena, R., Cronin, H., Dorey, R. & Silva, S. Direct current contact-mode triboelectric nanogenerators via systematic phase shifting. *Nano Energy* **75**, 104887 (2020).

46. Kim, T. et al. Direct-current triboelectric nanogenerator via water electrification and phase control. *Nano Energy* **52**, 95–104 (2018).
47. Li, M., Jiang, T., Ren, Y. & Jiang, H. Constant direct current triboelectric nanogenerator based on soft-contact mode for self-powered cathodic protection. *Nano Energy* **103**, 107777 (2022).
48. Tao, K. et al. Direct-current, long-lasting and highly efficient electret energy harvesting from ultra-low-frequency motions using toothed clutch mechanism. *Nano Energy* **105**, 107998 (2023).
49. Wu, Z. B. et al. Rotary disk multi-phase freestanding-electret generator with enhanced power and low ripple output. *Nano Energy* **83**, 105787 (2021).
50. Chen, P. F. et al. Rationally segmented triboelectric nanogenerator with a constant direct-current output and low crest factor. *Energy Environ. Sci.* **14**, 4523–4532 (2021).
51. Ryu, H. et al. Sustainable direct current powering a triboelectric nanogenerator via a novel asymmetrical design. *Energy Environ. Sci.* **11**, 2057–2063 (2018).
52. Li, H. et al. High power and low crest factor of direct-current triboelectric nanogenerator for self-powered optical computing system. *Energy Environ. Sci.* **16**, 4641–4649 (2023).
53. Wang, J. et al. High-performance and humidity-resistant direct-current triboelectric nanogenerator by coupling method combing charge excitation and phase shift. *Adv. Mater. Technol.* **8**, 2300480 (2023).
54. Li, X. Y. et al. A highly efficient constant-voltage triboelectric nanogenerator. *Energy Environ. Sci.* **15**, 1334–1345 (2022).
55. Hu, Y. X. et al. Triboelectric nanogenerator with low crest factor via precise phase difference design realized by 3D printing. *Small Methods* **5**, 2100936 (2021).
56. Hu, Y. X. et al. A noncontact constant-voltage triboelectric nanogenerator via charge excitation. *ACS Energy Lett.* **8**, 2066–2076 (2023).
57. Hu, Y. X. et al. A combined wind harvesting and speed sensing system based on constant-voltage triboelectric nanogenerator. *Adv. Energy Mater.* **14**, 2400672 (2024).
58. Li, X. Y. et al. Efficient energy transport in constant-voltage triboelectric nanogenerator-based power units. *Energy Environ. Sci.* **17**, 1244–1254 (2024).
59. Mao, X. et al. AI-driven ocean monitoring with multimodal triboelectric nanogenerator: Self-sustainable real-time wave warning and forecasting system. *Nano Energy* **140**, 111004 (2025).
60. Dong, Y. et al. Exploring human motions for smart wearables: energy conversion, harvesting and self–powered sensing. *Nano Energy* **143**, 111289 (2025).
61. Tao, K. et al. Development of bipolar-charged electret rotatory power generator and application in self-powered intelligent thrust bearing. *Nano Energy* **90**, 106491 (2021).
62. Wang, J. et al. Cylindrical direct-current triboelectric nanogenerator with constant output current. *Adv. Energy Mater.* **10**, 1904227 (2020).


## Acknowledgements

This work was supported by the National Key R & D Project from Minister of Science and Technology (2021YFA1201602), and the National Natural Science Foundation of China (No. U21A20147 and 62304024). W.J. discloses support for the research of this work from the National Key R & D Project from Minister of Science and Technology [2021YFA1201602], the National Natural Science Foundation of China [No. U21A20147]. L.X. discloses support for publication of this work from the National Natural Science Foundation of China [62304024].

## Author contributions

L.X. contributed to ideation, initial literature collection, original writing, editing, reviewing, and founding collection; Y.L. and L.P. contributed to initial literature collection; W.J. contributed to ideation, reviewing, supervision, and founding collection.

## Competing interests

The authors declare no competing interests.

## Additional information

**Supplementary information** The online version contains supplementary material available at https://doi.org/10.1038/s43246-026-01091-3.

**Correspondence** and requests for materials should be addressed to Jie Wang.

**Peer review information** *Communications Materials* thanks Hao Wu and the other, anonymous, reviewer(s) for their contribution to the peer review of this work. A peer review file is available.